arXiv:1704.06285v1 [cond-mat.quant-gas] 20 Apr 2017

Topological edge state manifestation of interacting 2D boson lattices in a harmonic trap

Bogdan Galilo,[1] Derek K. K. Lee,[2] and Ryan Barnett[1]
[1]*Department of Mathematics and* [2]*Blackett Laboratory,*
Imperial College London, London SW7 2AZ, United Kingdom
(Dated: April 24, 2017)

In this work, it is shown that interactions can facilitate the emergence of topological edge states of bosonic systems in the presence of a harmonic potential. This effect is demonstrated with the concrete model of a hexagonal lattice populated by spin-one bosons under a synthetic gauge field. In fermionic or non-interacting systems, the presence of a harmonic trap can obscure the observation of edge states. For our system with weakly interacting bosons in the Thomas-Fermi regime, we can clearly see a topological band structure with a band gap traversed by edge states. We also find that the number of edge states crossing the gap is increased in the presence of a harmonic trap, and the edge-modes experience an energy shift while traversing the first Brillouin zone which is related to the topological properties of the system. We find an analytical expression for the edge-state energies and our comparison with numerical computation shows excellent agreement.

Optical lattice experiments offer the possibility of simulating atomic crystal structures, creating a clean and well-controlled environment for probing many-body physics concepts and phenomena. In recent years, lattices reassembling the Hofstadter [1–3] and Haldane [4] models were created in optical lattice setups. A central focus in such systems lies in the manifestation of surface states which is a result of the non-trivial bulk topological properties. In topological insulators [5, 6], for instance, electron excitations form a Fermi sea and provided the Fermi level is within the band gap the near-equilibrium dynamics is dominated by the states localized either at the sharp boundaries or at the interface with a system of a different topology. However, unlike solids, ultracold atoms are typically confined by a harmonic trapping potential. The influence of the harmonic trap on the band structure and its topology is therefore of significant importance.

Theoretical studies suggest the presence of a confining potential can modify both the bulk and edge energy spectrum significantly, leading not only to a change in group velocity of edge modes but also to an emergence of additional edge states [7, 8], their disappearance [9], or localization and a shrinking of the bulk region [8, 10]. Possible ways of overcoming these difficulties include inducing topological interfaces [11, 12] and creating a confinement sharper than harmonic [8, 13, 14]. Creation of such trapping potentials represents a separate challenge and cost for experimental setup. The role of mean field interactions in the Haldane boson model was also considered in [15] where it was shown that the bulk gap can close when the harmonic trap is taken into account. We, however, show that an interacting gas of spin-one bosons prepared in a polar ground state on a two-dimensional lattice can have a clear gap in the energy spectrum of the spin-±1 excitations. Furthermore the gap is crossed by edge states that reflect the topological structure of the lattice.

Advances in the creation of synthetic gauge fields for atoms in optical lattices, as well as in photonic crystals have allowed the investigation of topological bands populated by bosons [16, 17]. Of particular relevance is the realisation of topological collective excitations in these systems [18–20]. While fermions form a Fermi sea, bosons tend to occupy the lowest energy state available and population of the higher energy edge modes is a challenge. Ways to overcome this challenge were suggested. In particular quantum quenches provide a tool to selectively induce dynamical instabilities in edge modes of topological bosonic systems [18] (quenches in similar fermionic systems were considered in [21]). The use of periodic driving has also been proposed [22–24]. In these studies, idealized (e.g. open) boundary conditions were adopted for simplicity.

In this manuscript, we show that pristine edge modes, much like those occurring in systems with idealised open boundary conditions, can occur in certain harmonically trapped interacting systems. In particular, interactions treated at the mean-field level can screen out the confining potential near the center of the trap, leading to an effectively flat potential. Additionally in a spinor system one can have pairing terms which are either small or zero near the center of the trap. We demonstrate that, with these combined ingredients, robust topological edge states can exist in the collective excitation spectrum of such a system when the bulk gap is larger than the characteristic energy scale $\gamma \sim M\omega^2 x_{\rm TF} a$ in the Thomas-Fermi regime where ω is the trapping frequency, M is the mass of the constituent bosons, $x_{\rm TF}$ is the Thomas-Fermi radius of the system, and a is the lattice constant. Additionally, for the case of γ much smaller than the band gap, we will derive an analytical expression for the edge state dispersion, which is also a central result of this work.

We focus on $S = 1$ spinor condensates on a lattice. We introduce boson spinor operators $\hat{\mathbf{\Psi}}_i = (\hat{\Psi}_{i,1}, \hat{\Psi}_{i,0}, \hat{\Psi}_{i,-1})^T$ and consider a spin-one generaliza-

tion of Kane-Mele model:

$$\hat{\mathcal{H}}_{\rm latt} = -w \sum_{\langle ij \rangle} \hat{\mathbf{\Psi}}_i^\dagger \hat{\mathbf{\Psi}}_j + i\lambda \sum_{\langle\langle ij \rangle\rangle} \nu_{ij} \hat{\mathbf{\Psi}}_i^\dagger S_z \hat{\mathbf{\Psi}}_j, \quad (1)$$

where we denote the 3×3 spin-one matrices as $\mathbf{S} = (S_x, S_y, S_z)$ and the tunneling towards the left (right) next nearest-neighbor site is determined by $i\lambda\nu_{ij} = +i(-i)\lambda$ [25]. Although we expect the results of the current work to exist for other models, we concentrate on (1) to be concrete, and because we considered this model in a previous work [18]. The model exhibits two bands for each spin component. The next-nearest-neighbor term vanishes for spin 0 components and the Hamiltonian reduces to graphene model. The other two spin components each have a gap of 4λ in energy spectrum, closed only by chiral topological edge modes. In the following, we will write this model more compactly as $\hat{\mathcal{H}}_{\rm latt} = \sum_{ij} \hat{\mathbf{\Psi}}_i^\dagger \mathcal{H}_{\rm latt}^{ij} \hat{\mathbf{\Psi}}_j$ where the $\mathcal{H}_{\rm latt}^{ij}$ matrix can be directly determined from (1).

Since we are mainly interested in the manifestation of edge modes, we will consider the strip geometry. We keep the lattice periodicity along $\mathbf{a}_1$ primitive lattice vector, while considering harmonic trapping confinement in the perpendicular direction given by:

$$\hat{V}_\omega = \sum_j \frac{M\omega^2 x_j^2}{2} \hat{\rho}_j, \quad (2)$$

where ω is the confining frequency, $\hat{\rho}_j = \hat{\mathbf{\Psi}}_j^\dagger \hat{\mathbf{\Psi}}_j$ is the local number operator and x_j is the location of the j-th site with respect to the center of the trap taken along the x-direction as depicted in Fig. 1.

We now include on-site interactions terms that do not break spin rotational symmetry:

$$\hat{\mathcal{H}}_{\rm int} = \sum_j \frac{U}{2} \hat{\rho}_j^2 + \frac{U_S}{2} \hat{\mathbf{S}}_j^2, \quad (3)$$

where $\hat{\mathbf{S}}_j = \hat{\mathbf{\Psi}}_j^\dagger \mathbf{S} \hat{\mathbf{\Psi}}_j$ is the local spin operator. We also consider a quadratic Zeeman term $\hat{\mathcal{H}}_Z = q_Z \sum_j \hat{\mathbf{\Psi}}_j^\dagger S_z^2 \hat{\mathbf{\Psi}}_j$ which is experimentally adjustable using external magnetic fields or microwave fields [26]. The linear Zeeman term is omitted due to the S_z symmetry of our model. We require a positive q_Z in order to ensure the ground state is a spin-0 boson state. The total Hamiltonian now reads:

$$\hat{\mathcal{H}} = \hat{\mathcal{H}}_{\rm latt} + \hat{\mathcal{H}}_{\rm int} + \hat{\mathcal{H}}_Z + \hat{V}_\omega - \mu \sum_j \hat{\rho}_j, \quad (4)$$

where μ is the chemical potential.

At low enough temperatures atoms occupy the ground state $\bar{\mathbf{\Psi}}_j$, which we treat classically. For sufficiently large and positive q_Z, the ground state is a polar state where $\bar{\mathbf{S}}_j = \bar{\Psi}_j^\dagger \mathbf{S} \bar{\Psi}_j = 0$ and $\bar{\mathbf{\Psi}}_j = (0, \sqrt{\bar{\rho}_j}, 0)^T$. We consider a slowly varying confining potential, much slower than the lattice characteristic length scale, so the ground state population extends over a considerable number of lattice sites. Provided the density and spin fluctuations,

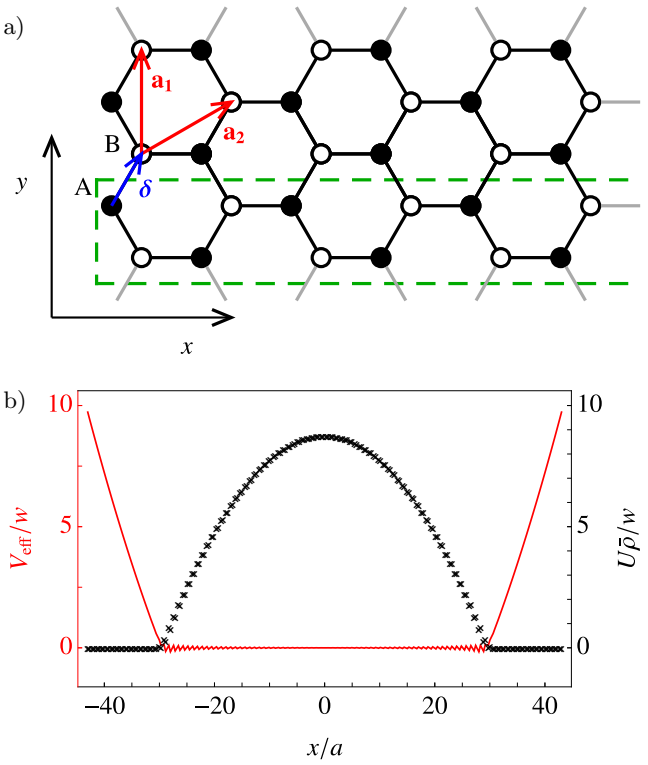

FIG. 1. a) Lattice structure, determined by the primitive lattice vectors $\mathbf{a}_1$ and $\mathbf{a}_2$ of length a. Closed and open circles denote the triangular sublattice sites A and B respectively. We consider a strip geometry with open (periodic) boundary conditions in $x(y)$-direction. b) The effective potential $V_{\rm eff}$ (red solid line) and the density profile of the ground state $U\bar{\rho}$ (black cross marks). These quantities are obtained numerically and are in excellent agreement with the Thomas-Fermi profile. Here $\lambda = w/2$, $M\omega^2 a^2 = 0.02w$ and $UN_{\rm str} = 800w$, where $N_{\rm str}$ is the total number of bosonic particles in a strip denoted by the (green) dashed lines in (a).

$\delta\hat{\rho} = \hat{\rho} - \bar{\rho}$ and $\delta\hat{\mathbf{S}} = \hat{\mathbf{S}} - \bar{\mathbf{S}}$, are small, the fluctuations about the ground state $\hat{\boldsymbol{\psi}} = \hat{\mathbf{\Psi}} - \bar{\mathbf{\Psi}}$ up to quadratic order are described by the Bogoliubov-de Gennes (BdG) Hamiltonian:

$$H_{\rm B} = \sum_{ij} \hat{\boldsymbol{\psi}}_i^\dagger \left(\mathcal{H}_{\rm latt}^{ij} - \delta_{ij} \bar{\mathcal{H}}_{\rm latt} \right) \hat{\boldsymbol{\psi}}_j + \sum_j V_{{\rm eff},j} \hat{\boldsymbol{\psi}}_j^\dagger \hat{\boldsymbol{\psi}}_j + \sum_j q_Z \hat{\boldsymbol{\psi}}_j^\dagger S_z \hat{\boldsymbol{\psi}}_j + \frac{U}{2} \delta\hat{\rho}_j^2 + \frac{U_S}{2} \delta\hat{\mathbf{S}}_j^2, \quad (5)$$

where we have introduced the mean kinetic energy per particle in the condensate $\bar{\mathcal{H}}_{\rm latt} = \sum_{i,j} \bar{\mathbf{\Psi}}_i^\dagger \mathcal{H}_{\rm latt}^{ij} \bar{\mathbf{\Psi}}_j / \sum_{j'} \bar{\rho}_{j'}$ and the effective potential:

$$V_{{\rm eff},j} = M\omega^2 x_j^2/2 + \bar{\mathcal{H}}_{\rm latt} + U\bar{\rho}_j - \mu. \quad (6)$$

Prior to evaluating the fluctuation modes of the BdG Hamiltonian, we first discuss the effect of screening of confining potential. The ground state density profile $\bar{\mathbf{\Psi}}$ is determined by the time-independent Gross-Pitaevskii

equation:

$$\sum_j \left(\mathcal{H}^{ij}_{\rm latt} - \bar{\mathcal{H}}_{\rm latt}\delta_{ij} + V_{{\rm eff},i}\delta_{ij} \right) \bar{\mathbf{\Psi}}_j = 0. \qquad (7)$$

At large distances from the center of the trap the population density $\bar{n}_j$ vanishes and the confining potential takes the leading role in $V_{\rm eff}$. On the other hand, for distances closer to the center of the trap, the ground state population is larger. Under the Thomas-Fermi approximation for the mean-field density, applicable when $\sqrt{M\omega^2 a^2 w} \ll U \max_j \bar{\rho}_j$, the effective potential $V_{\rm eff}$ indeed will vanish identically inside the Thomas-Fermi radius given by $x_{TF} = \sqrt{2(\mu - \bar{\mathcal{H}}_{\rm latt})/(M\omega^2)}$. Shown in Fig.1 is the effective potential which is computed numerically and demonstrates the statements above. Such a screening occurs in standard scalar BECs. In this sense, interactions contribute to the screening of the harmonic trap inside the Thomas-Fermi region. Deviations from the Thomas-Fermi approximation can be seen around the Thomas-Fermi radius. These are due to the fast variations within the unit cell that are not perfectly screened.

We now turn to the discussion of the fluctuation spectrum of the BdG Hamiltonian (5), which is the central focus of this work. Due to S_z symmetry the spin-±1 components decouple from the spin-0 ones in $\mathcal{H}_B$. The density fluctuation term in (5) carries only spin-0 components $\delta\hat{\rho}^2_j = \bar{\rho}_j(\hat{\psi}^\dagger_{j,0}\hat{\psi}_{j,0} + \hat{\psi}_{j,0}\hat{\psi}_{j,0} + \text{H.c.})$, while the spin fluctuation term couples the spin-±1 components: $\delta\hat{\mathbf{S}}^2_j = \bar{\rho}_j(\hat{\psi}^\dagger_{j,+1}\hat{\psi}_{j,+1} + \hat{\psi}^\dagger_{j,-1}\hat{\psi}_{j,-1} + \hat{\psi}_{j,+1}\hat{\psi}_{j,-1} + \hat{\psi}^\dagger_{j,+1}\hat{\psi}^\dagger_{j,-1} + \text{H.c.})$. In typical spinor condensates, the spin-spin interaction is much smaller than the density-density interaction. For instance, for ^{87}Rb, U_S will be two orders of magnitude smaller than U. For this case, the Hamiltonian describing the ±1 components will be, to a good approximation, translationally invariant within the Thomas-Fermi radius. An interface is then encountered at $x = x_{TF}$, where the effective potential rises (Fig. 1) and the system loses its translational invariance. Similar approximations have previously been employed to simplify the computation of the spatial structure of parametrically amplified spin modes [27].

To better understand the effect of trap screening on the manifestation of topological edge modes, we now turn to an effective description of the edge state emergence around the screening boundaries outside the Thomas-Fermi radius. As the edge states are composed entirely of ±1 components, we will restrict our attention to these modes. Outside of the Thomas-Fermi radius, we may neglect the last two terms in (5) as the mean-field particle density vanishes in this region, so that pairing terms are absent. We assume the boundary region to be sufficiently small in comparison to the lattice constant induced by optical lattice potential and will discuss the effect of these restrictions later.

In the following, we will describe a fairly general method to compute the dispersion of edge modes in a soft potential, but will give quantities relevant to our particular model in the Supplemental Material. Note that outside the Thomas-Fermi radius, the effective potential reduces to the trapping potential, and interactions are unimportant since the mean-field density vanishes in this region. As a result the spin components decouple and without loss of generality we will focus on one spin component. Let k denote the wave number along the $\mathbf{a}_1$ periodic direction and n label the unit cell along the $\mathbf{a}_2$ lattice vector. The two sublattices of our model are spatially separated and consequently the corresponding atoms at the same n-th unit cell experience a different magnitude of the confining potential. While the excitations related to one sublattice experience an effective potential $\mathcal{V}(n)$, the excitations related to the other sublattice experience a potential $\mathcal{V}(n+s)$, where s accounts for the relative lattice separation. For the specific model (1) of this manuscript, $s = 1/3$ [28]. The energy spectrum of the system outside of the Thomas-Fermi radius is given by the eigenvalues E_k of a difference equation of the form:

$$\sum_{n'} H_{k,n-n'}\mathbf{\Phi}_{k,n'} + V_n\mathbf{\Phi}_{k,n} = E_k\mathbf{\Phi}_{k,n}, \qquad (8)$$

where $H_{k,n-n'}$ and $V_n = \text{diag}(\mathcal{V}(n), \mathcal{V}(n+s))$ are 2×2 matrices corresponding to the sublattice degrees of freedom [28] (the treatment can also be generalized to larger matrices). In (8), $H_{k,n-n'}$ follows from $\mathcal{H}^{ij}_{\rm latt}$ while V_n

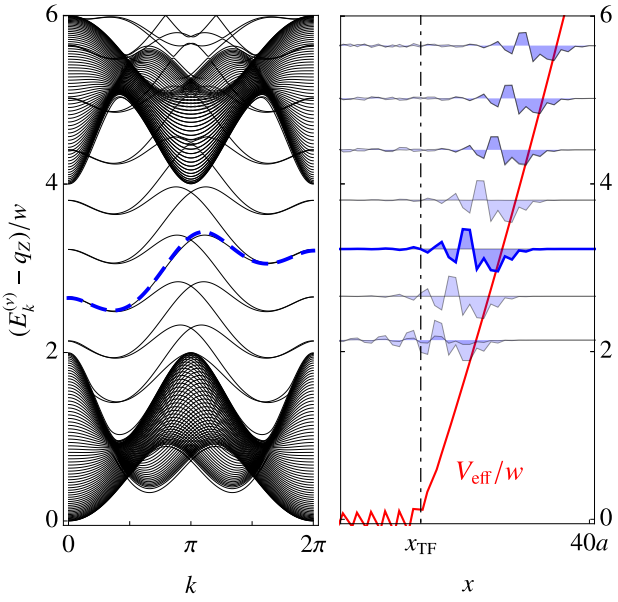

FIG. 2. Left: The energy spectrum corresponding to the spin-$1(-1)$ excitations. The solid lines correspond to numerical results, while the dashed line corresponds to the analytical expression (13) for a particular mode. Right: The effective potential in units of w near the Thomas-Fermi radius $x_{\rm TF}$ (red) and the wave functions of the eigen-modes in arbitrary units at $k = 2\pi$ (blue). Here $\lambda = w/2$, $M\omega^2a^2 = 0.02w$ and $UN_{\rm str} = 800w$.

follows from the effective potential (6).

We consider a lattice point $\bar{n}$ outside of the Thomas-Fermi radius and expand about it to first order: $V_n = V_{\bar{n}} + V'_{\bar{n}}(n-\bar{n})$. We will search for solutions localized about $\bar{n}$. Such an approximation is valid since the effective potential is nearly linear in this region (see Fig. 1). We next Fourier transform (8) under this approximation to obtain

$$E_k \mathbf{\Phi}_{k,\varphi} = \left[H_{k,\varphi} + V_{\bar{n}} + V'_{\bar{n}}(i\partial_\varphi - \bar{n})\right] \mathbf{\Phi}_{k,\varphi} \tag{9}$$

where $H_{k,\varphi} = \sum_n e^{-i(n-n')\varphi} H_{k,n-n'}$ and $\mathbf{\Phi}_{k,\varphi} = \sum_n e^{-in\varphi}\mathbf{\Phi}_{k,\varphi}$. With these relations, we see that both $H_{k,\varphi}$ and $\mathbf{\Phi}_{k,\varphi}$ are necessarily 2π-periodic in φ. The following analysis is simplified by performing a unitary transformation so that matrices corresponding to the potential in the above are made to be proportional to the identity matrix. Such a transformation is achieved by $\mathcal{U}_\varphi = \mathrm{diag}(1, e^{is\varphi})$. Under this transformation, (9) becomes

$$i\gamma_{\bar{n}}\partial_\varphi \tilde{\mathbf{\Phi}}_{k,\varphi} = (E_k - \tilde{H}_{k,\varphi} - \tilde{V}_{\bar{n}} + \mathbb{1}\bar{n}\gamma_{\bar{n}})\tilde{\mathbf{\Phi}}_{k,\varphi} \tag{10}$$

where $\tilde{\mathbf{\Phi}}_{k,\varphi} = \mathcal{U}^\dagger_\varphi \mathbf{\Phi}_{k,\varphi}$, $\tilde{H}_{k,\varphi} = \mathcal{U}^\dagger_\varphi H_{k,\varphi}\mathcal{U}_\varphi$, $\tilde{V}_{\bar{n}} = \mathcal{V}(\bar{n})\mathbb{1}$, and $\gamma_{\bar{n}} = \mathcal{V}'(\bar{n})$. The solution to this is readily found to be

$$\tilde{\mathbf{\Phi}}_{k,\varphi} = e^{-i\left(\bar{n}+\frac{E_k-\mathcal{V}(\bar{n})}{\gamma_{\bar{n}}}\right)\Delta\varphi}\mathcal{P}e^{\frac{i}{\gamma_{\bar{n}}}\int_{\varphi_0}^{\varphi} d\varphi'\, \tilde{H}_{k,\varphi'}}\tilde{\mathbf{\Phi}}_{k,\varphi_0}. \tag{11}$$

Here $\mathcal{P}$ is the path ordering operator for φ and $\Delta\varphi = \varphi - \varphi_0$ where φ_0 is arbitrary. Note that the eigenvalues of $\tilde{H}_{k,\varphi}$ give the bulk band dispersions in the non-interacting limit.

For the case when $\gamma_{\bar{n}}$ is significantly smaller than the eigenvalue spacing of $\tilde{H}_{k,\varphi}$, i.e. much smaller than the bulk band gap, the adiabatic approximation can be used. To do so, we introduce the 'instantaneous' eigenbasis: $\tilde{H}_{k,\varphi}\tilde{\boldsymbol{\phi}}^{(\nu)}_{k,\varphi} = \varepsilon^{(\nu)}_{k,\varphi}\tilde{\boldsymbol{\phi}}^{(\nu)}_{k,\varphi}$ where ν labels the eigenvectors/eigenenergies and let $\boldsymbol{\phi}^{(\nu)}_{k,\varphi} = \mathcal{U}_\varphi\tilde{\boldsymbol{\phi}}^{(\nu)}_{k,\varphi}$. Here, $\varepsilon^{(\nu)}_{k,\varphi}$ are the bulk eigenstates of the non-interacting infinite system. Invoking the adiabatic approximation, and transforming back to the original variables, one finds

$$\mathbf{\Phi}_{k,\varphi} = e^{-i\left(\bar{n}+\frac{E_k-\mathcal{V}(\bar{n}+\frac{s}{2})}{\gamma_{\bar{n}}}\right)\Delta\varphi} \times \sum_\nu e^{i\int_{\varphi_0}^{\varphi} d\varphi'\left(\frac{\varepsilon^{(\nu)}_{k,\varphi'}}{\gamma_{\bar{n}}}+A^{(\nu)}_{k,\varphi'}-\frac{sZ^{(\nu)}_{k,\varphi'}}{2}\right)}\left[\boldsymbol{\phi}^{(\nu)\dagger}_{k,\varphi_0}\mathbf{\Phi}_{k,\varphi_0}\right]\boldsymbol{\phi}^{(\nu)}_{k,\varphi} \tag{12}$$

where $A^{(\nu)}_{k,\varphi} = i\boldsymbol{\phi}^{(\nu)\dagger}_{k,\varphi}\partial_\varphi\boldsymbol{\phi}^{(\nu)}_{k,\varphi}$ is the Berry connection and $Z^{(\nu)}_{k,\varphi} = \boldsymbol{\phi}^{(\nu)\dagger}_{k,\varphi}\sigma_z\boldsymbol{\phi}^{(\nu)}_{k,\varphi}$ (σ_z is a Pauli matrix).

Requiring $\mathbf{\Phi}_{k,\varphi}$ to be 2π-periodic in φ, enables one to determine the energies E_k entering (12). Labeling these as $E^{(\bar{n}\nu)}_k$, one finds

$$E^{(\bar{n}\nu)}_k = \mathcal{V}\left(\bar{n}+\frac{s}{2}\right) + \frac{1}{2\pi}\int_0^{2\pi} d\varphi\left(\varepsilon^{(\nu)}_{k,\varphi} + \gamma_{\bar{n}}A^{(\nu)}_{k,\varphi} - \frac{s\gamma_{\bar{n}}}{2}Z^{(\nu)}_{k,\varphi}\right). \tag{13}$$

Different values of $\bar{n}$ correspond to edge states localized at different places along along the x-direction. This expression is remarkable in that it expresses the edge state dispersion purely in terms of the external potential and basic quantities of the bulk system. The (integer) Chern numbers of the bulk system are given by

$$\mathcal{C}_\nu = \frac{1}{2\pi}\int_0^{2\pi} d\varphi \int_0^{2\pi} dk\ \Omega^{(\nu)}_{k,\varphi}, \tag{14}$$

where $\Omega^{(\nu)}_{k,\varphi} = i\left(\partial_k\boldsymbol{\phi}^{(\nu)\dagger}_{k,\varphi}\partial_\varphi\boldsymbol{\phi}^{(\nu)}_{k,\varphi} - \partial_\varphi\boldsymbol{\phi}^{(\nu)\dagger}_{k,\varphi}\partial_k\boldsymbol{\phi}^{(\nu)}_{k,\varphi}\right)$ is the Berry curvature. Using this and (13), one sees that the edge state band energies change by $\gamma_{\bar{n}}\mathcal{C}_\nu$ as the one-dimensional Brillouin zone is traversed: $\Delta E^{(\bar{n}\nu)}_k = E^{(\bar{n}\nu)}_{k=2\pi} - E^{(\bar{n}\nu)}_{k=0} = \gamma_{\bar{n}}\mathcal{C}_\nu$.

A result similar to (13) was previously uncovered in [29], though the methods used there are rather different from those used presently. The work [29] considered a topological system under a strictly linear external field, the so-called Wannier-Stark ladder. A semiclassical theory of the system was developed using the methods of [30]. The theory was quantized by the Bohr-Sommerfeld condition to deduce the eigenenergies. Our expression (13) reduces to the result of [29] in the limit when $\mathcal{V}_{\bar{n}}$ is a strictly linear potential and the external field couples identically to sites with the same n (i.e. $s = 0$).

We support our results by performing numerical computations. We evolve the Gross-Pitaevskii equation (7) in imaginary time to find the ground state in the Thomas-Fermi regime. We then compute the collective spin excitations. Comparison with the analytical result (13) shows excellent agreement (see Fig. 2). Deviations from (13) do occur for the edge states with energies close to the corresponding bulk band from which they emerge. For these energy levels the overlap between states (12) and bulk states cannot be ignored. The focus of this manuscript, however, lies in describing the emergence of topological edge states with energies well within the gap and/or outside the bulk bands. Nevertheless, we point out that our method can be improved by requiring corresponding matching conditions at the screening radius and retaining higher order derivatives of the confining potential. We also find that the degeneracy of the edge states changes depending on its energy. As can be seen in Fig. 2 the chiral edge states can pass through a given energy level several times. However, the difference between the number of right and left movers, N^ν_R and N^ν_L correspondingly, at the same energy level is fixed by the topological structure of the bulk states: $N^\nu_R - N^\nu_L = C_\nu$. This is a direct indication of the topological nature of the bulk states and a consequence of the bulk-boundary correspondence [5, 6].

In summary, despite harmonic confinement being known for obscuring observation of topological edge-states we have shown that interactions can facilitate the emergence of these states in topological lattices populated by a spinor Bose condensate. In the Thomas-Fermi regime sharp boundaries emerge due to the screening of

the harmonic trap inside the Thomas-Fermi radius. We have found localized states emerging outside the Thomas-Fermi radius. We have also shown that these states carry information about the lattice topology inside the screening radius. Our results are valid both for antiferromagnetic ($U_s > 0$) and ferromagnetic ($U_s < 0$) interactions. Our analysis gives new insight into the emergence of topological edge states at soft boundaries and opens new doors in the exploration of topological properties in optical lattice experiments with spin-1 bosons.

The authors would like to acknowledge Ari Turner for useful discussions. We are grateful for support from the Schrodinger Scholarship Scheme at Imperial College London (B. G.); the European Union's Seventh Framework Programme for Research, Technological Development, and Demonstration under Grant No. PCIG-GA-2013-631002 and the Aspen Center for Physics under Grant No. PHYS-1066293 (R. B.)

Appendix A: Supplemental material

Here we unveil the quantities used in (8) and thereafter in correspondence to the Kane-Mele model. Since in the region outside the Thomas-Fermi radius the system is effectively non-interacting the spin components decouple. Below we describe only the spin $m = 1$ component. The other two components $m = -1$ and $m = 0$ can be related to the $m = 1$ case by setting $\lambda \to -\lambda$ and $\lambda \to 0$ with $q_Z \to 0$ respectively. The Hamiltonian matrix $H_{k,n-n'}$ for the spin $m = 1$ component is given by

$$H_{k,n-n'} = R_k \delta_{n-n',0} + M_k \delta_{n-1,n'} + M_k^\dagger \delta_{n+1,n'}, \quad \text{(A1)}$$

where R_k and M_k are 2×2 matrices acting on the sublattice indices and are given by

$$R_k = \begin{pmatrix} 2\lambda \sin k & -w(1+e^{-ik}) \\ -w(1+e^{ik}) & -2\lambda \sin k \end{pmatrix}, \quad \text{(A2)}$$

$$M_k = \begin{pmatrix} i\lambda(1-e^{-ik}) & 0 \\ -w & i\lambda(1-e^{-ik}) \end{pmatrix}. \quad \text{(A3)}$$

Switching from $n - n'$ to its conjugate φ and introducing Pauli matrices σ_1, σ_2, and σ_3 reduces the Hamiltonian matrix to

$$H_{k,\varphi} = d_1\sigma_1 + d_2\sigma_2 + d_3\sigma_3,$$

where $d_1 = -w(1 + \cos k + \cos\varphi)$, $d_2 = -w(\sin k + \sin\varphi)$ and $d_3 = -2\lambda(\sin\varphi - \sin(\varphi - k) - \sin k)$. The above Hamiltonian has two eigenvalues $\epsilon^{(\pm)}_{k,\varphi} = \pm\sqrt{d_1^2 + d_2^2 + d_3^2} = \pm d$ and the corresponding eigenvectors can be written as

$$\phi^{(\pm)}_{k,\varphi} = \left(\frac{d \pm d_3}{\sqrt{2d(d \pm d_3)}}, \pm \frac{d_1 + id_2}{\sqrt{2d(d \pm d_3)}} \right)^{\mathrm{T}}. \quad \text{(A4)}$$

It is then straightforward to find an expression for the Berry connection $A^{(\nu)}_{k,\varphi} = i\boldsymbol{\phi}^{(\nu)\dagger}_{k,\varphi} \partial_\varphi \boldsymbol{\phi}^{(\nu)}_{k,\varphi}$ (in a particular gauge):

$$A^{(\nu)}_{k,\varphi} = \frac{-w^2\,(1 + \cos\varphi + \cos(\varphi - k))}{2\epsilon^{(\nu)}_{k,\varphi}\left[\epsilon^{(\nu)}_{k,\varphi} - 2\lambda\,(\sin\varphi - \sin(\varphi - k) - \sin k)\right]}. \quad \text{(A5)}$$

This term causes the edge states to experience a shift in energy while wrapping them around the first Brillouin zone. There is also a term caused by the non-linearity of the potential:

$$Z^{(\nu)}_{k,\varphi} = d_3(k,\varphi)/\epsilon^{(\nu)}_{k,\varphi}. \quad \text{(A6)}$$

The trapping potential also lifts the energies of the edge mode excitations localized about lattice site $\bar{n}$. For reasons of computational convenience we have considered the trapping potential to be oriented in the direction perpendicular to the primitive lattice vector $\mathbf{a}_1$. Thus the excitations within the sublattice A experience a harmonic potential $\mathcal{V}(n) = M\omega^2 n^2(\mathbf{a}_2 \cdot \hat{\mathbf{x}} - x_c)^2/2 + q_Z - \mu$ centered at position $x_c = (\mathbf{a}_2 \cdot \hat{\mathbf{x}})(N + 1 + s)/2$ and shifted by the chemical potential μ and quadratic Zeeman coupling q_Z, where $2N$ is the total number of sites in a unit cell strip highlighted in Fig. 6. The sites of sublattice B, however, are displaced by a vector $\boldsymbol{\delta}$ and consequently experience a slightly different magnitude of the harmonic trap $\mathcal{V}(n + s)$. The value of the shift s accounts for the displacement $\boldsymbol{\delta}$ and is related to the primitive lattice vectors $\mathbf{a}_1$ and $\mathbf{a}_2$. We find

$$s = \frac{\mathbf{a}_1^2(\boldsymbol{\delta} \cdot \mathbf{a}_2) - (\mathbf{a}_1 \cdot \mathbf{a}_2)(\boldsymbol{\delta} \cdot \mathbf{a}_1)}{\mathbf{a}_1^2\mathbf{a}_2^2 - (\mathbf{a}_1 \cdot \mathbf{a}_2)^2}. \quad \text{(A7)}$$

For the hexagonal lattice considered in this manuscript, $s = 1/3$.

[1] R. A. Williams, S. Al-Assam, and C. J. Foot, Phys. Rev. Lett. **104**, 050404 (2010).

[2] M. Aidelsburger, M. Atala, M. Lohse, J. T. Barreiro, B. Paredes, and I. Bloch, Phys. Rev. Lett. **111**, 185301 (2013).

[3] H. Miyake, G. A. Siviloglou, C. J. Kennedy, W. C. Burton, and W. Ketterle, Phys. Rev. Lett. **111**, 185302 (2013).

[4] G. Jotzu, M. Messer, R. Desbuquois, M. Lebrat, T. Uehlinger, D. Greif, and T. Esslinger, Nature **515**, 237 (2014).

[5] M. Z. Hasan and C. L. Kane, Rev. Mod. Phys. **82**, 3045 (2010).

[6] X.-L. Qi and S.-C. Zhang, Rev. Mod. Phys. **83**, 1057

(2011).
[7] T. D. Stanescu, V. Galitski, and S. Das Sarma, Phys. Rev. A **82**, 013608 (2010).
[8] M. Buchhold, D. Cocks, and W. Hofstetter, Phys. Rev. A **85**, 063614 (2012).
[9] Z. Yan, B. Li, X. Yang, and S. Wan, Scientific Reports **5**, 16197 EP (2015).
[10] A. R. Kolovsky, F. Grusdt, and M. Fleischhauer, Phys. Rev. A **89**, 033607 (2014).
[11] N. Goldman, G. Jotzu, M. Messer, F. Grg, R. Desbuquois, and T. Esslinger, arXiv:1606.00015 (2016).
[12] M. Leder, C. Grossert, L. Sitta, M. Genske, A. Rosch, and M. Weitz, arXiv preprint arXiv:1604.02060 (2016).
[13] A. L. Gaunt, T. F. Schmidutz, I. Gotlibovych, R. P. Smith, and Z. Hadzibabic, Phys. Rev. Lett. **110**, 200406 (2013).
[14] L. Chomaz, L. Corman, T. Bienaimé, R. Desbuquois, C. Weitenberg, S. Nascimbène, J. Beugnon, and J. Dalibard, Nat. Commun. **6**, 6162 (2015).
[15] S. Furukawa and M. Ueda, New Journal of Physics **17**, 115014 (2015).
[16] N. Goldman, G. Juzeliūnas, P. Ohberg, and I. B. Spielman, Reports on progress in physics. Physical Society (Great Britain) **77**, 126401 (2014).
[17] L. Lu, J. D. Joannopoulos, and M. Soljačić, Nature Photonics **8**, 821 (2014).
[18] B. Galilo, D. K. K. Lee, and R. Barnett, Phys. Rev. Lett. **115**, 245302 (2015).
[19] C.-E. Bardyn, T. Karzig, G. Refael, and T. C. Liew, Physical Review B **93**, 020502 (2016).
[20] V. Peano, M. Houde, C. Brendel, F. Marquardt, and A. A. Clerk, Nature communications **7** (2016).
[21] M. Caio, N. Cooper, and M. Bhaseen, arXiv preprint arXiv:1504.01910 (2015).
[22] G. Engelhardt, M. Benito, G. Platero, and T. Brandes, Phys. Rev. Lett. **117**, 045302 (2016).
[23] H. Dehghani and A. Mitra, Phys. Rev. B **93**, 205437 (2016).
[24] V. Peano, M. Houde, C. Brendel, F. Marquardt, and A. A. Clerk, Nat Commun **7** (2016), article.
[25] C. L. Kane and E. J. Mele, Phys. Rev. Lett. **95**, 146802 (2005).
[26] F. Gerbier, A. Widera, S. Fölling, O. Mandel, and I. Bloch, Phys. Rev. A **73**, 041602 (2006).
[27] M. Scherer, B. Lücke, G. Gebreyesus, O. Topic, F. Deuretzbacher, W. Ertmer, L. Santos, J. J. Arlt, and C. Klempt, Phys. Rev. Lett. **105**, 135302 (2010).
[28] See Supplemental Material at [URL will be inserted by publisher].
[29] W.-R. Lee and K. Park, Phys. Rev. B **92**, 195144 (2015).
[30] G. Sundaram and Q. Niu, Phys. Rev. B **59**, 14915 (1999).